THE JOURNAL OF PHYSICAL CHEMISTRY C

ARTICLE

pubs.acs.org/JPCC

Electrochemical Behavior and Magnetic Properties of Vanadium Oxide Nanotubes

Andreia I. Popa,*[,†] Evgenia Vavilova,[†,‡] Christine Täschner,[†] Vladislav Kataev,[†] Bernd Büchner,[†] and Rüdiger Klingeler[†,§]

[†]Leibniz Institute for Solid State and Materials Research, IFW Dresden, 01171 Dresden, Germany

[‡]Zavoisky Physical-Technical Institute of RAS − 420029, Kazan, Russia

[§]Kirchhoff Institute for Physics, University of Heidelberg, INF 227, 69120 Heidelberg, Germany

ABSTRACT: The electrochemical behavior and magnetic properties of electrochemically lithium-doped mixed valence vanadium oxide nanotubes (VOx-NTs) have been studied. The materials were synthesized hydrothermally. Primary amines ($CH_3-(CH_2)_{11}-NH_2$) were used as spacer molecules aiding to retain the nanotubular shape of the VOx layers. Cyclic voltammograms and potentiostatic measurements indicate that the electrochemical behavior of this material is fairly sensitive to the preparation conditions. Specific capacity values for this material are higher than similar template VOx-NTs. Lithium doping level of $x = 0.1$ in two different VOx-NTs gives rise to room-temperature ferromagnetism in Li_xVOx-NTs.

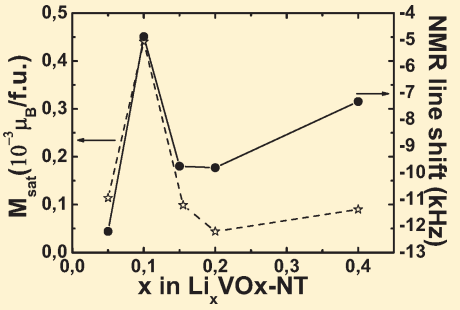

1. INTRODUCTION

In recent years, it turned out that nanoscaled materials can yield improved performance when used in electrodes of energy conversion devices, for example, batteries. For example, electrodes made of nanoparticles of transition metal oxides such as CoO, NiO, CuO, or FeO exhibit electrochemical capacities of 700 mAh/g with 100% capacity retention for up to 100 cycles and high recharging rates.[1]

The particular advantage of nanoparticle-based electrodes includes shorter lithium diffusion lengths and higher surface area than in micrometer electrode materials that leads to performance improvement of lithium-ion batteries.[2,3]

Among nanostructured materials those with tubular morphology are of large interest due to size-induced properties and complex nanoscale architecture.[4−6] In this context, self-organized oxide nanostructures provide a promising approach. Inorganic nanostructures such as TiS_2, SnO_2, or $MoS_{2-x}I_y$ with $x \approx 0$ and $y \approx 0.3$ have been studied in terms of battery application.[7,8] TiO_2 represents nowadays a powerful candidate for this application as well.[9] In this paper, we focus on self-assembled vanadium oxide (VOx) nanostructures synthesized for the first time by Spahr et al.[10] In general, VOx can be found in many forms and can have many and very different chemical or physical properties, in particular when different oxidation states of the vanadium ions are realized. The nanotubular modification that is addressed here can be synthesized only when organic spacer molecules are applied. Such spacer molecules can be for example primary amines or diamines, helping to retain the nanotube shape of the VOx layers. To be specific, VOx nanotubes can have diameters of 15−150 nm, tunnel openings between 5 and 50 nm, and lengths up to 15 μm. The nanotubes are formed by rolled VOx layers that show similarities with $BaV_7O_{16}\cdot nH_2O$, where $n = 4.4$. In this material, V_7O_{16} layers are stacked along one direction with Ba^{2+} ions and H_2O molecules located in between the layers. Analogously, the VOx nanotubes are formed by similar layers with the above-mentioned organic spacers placed in between. There can be 2−30 layers of VOx forming either tubular or spiral structures.[10−12] The organic molecules do not only affect the morphology of the nanotubes but also their electronic properties since the oxidation state of the vanadium ions is influenced.[13] In addition, the amines embedded between crystalline VOx layers can be exchanged by various metal cations, such as alkaline, alkaline-earth, or transition metals, without destroying the nanotubular shape but influencing their electrochemical properties.[10,14−16]

To assess possible applications of this material in lithium battery technology,[17] several electrochemical studies have been performed explicitly on ion-exchanged VOx-NT. For example, $Mn_{0.1}VO_{2.5}\cdot nH_2O$ was reversibly intercalated/deintercalated with Li and the material shows a specific capacity of 140 mAh/g.[15] Mo-doped tubes have an initial specific capacity of 200 mAh/g that drops to half after 50 cycles.[18] Na^+, Ca^+, and K^+ were as well successfully embedded between VOx layers. All of these have shown good electrochemical properties with averaged specific capacities around 150 mAh/g over 100 cycles.[16] The structural defects are also relevant in electrochemical properties of such materials. It has been shown that defect rich VOx nanorolls exhibit superior electrochemical properties compared

Received: September 29, 2010
Revised: February 1, 2011
Published: March 07, 2011

to well-ordered material with specific capacities of approximately 300 mAh/g.[19] These values already approach the theoretical capacity for exchanged nanotubes that amounts to about 370 mAh/g when all vanadium is reduced to V^{3+}. This extreme case is however unlikely because total reduction of V^{5+} to V^{3+} would induce strong structural deformations (collapsing) of the VOx-NT structure.[20]

Besides studying the applicability of VOx-NTs as electrode materials in lithium ion batteries, their electronic properties have been studied both in the pristine material[11,21,22] and after lithium doping.[21,23,24] By doping the VOx-NTs with either electrons[21,24] or holes,[21] a nonlinear field dependence of the magnetization is observed at room temperature. This surprising ferromagnetic-like response renders VOx-NTs a novel type of self-assembled nanoscaled magnets.

In this work, both the electrochemical performance and the effect of Li-intercalation on the magnetic properties of hydrothermally synthesized VOx-NTs have been studied. For this purpose, cyclic voltammetry and potentiostatic measurements have been performed. Using these electrochemical methods, it has been found that the electrochemical properties of similarly synthesized nanotubes differ from each other. Most probably these differences arise from influence of amines used during synthesis of the nanotubes. In addition, the effect of lithium doping on the magnetic properties of VOx-NTs has been studied after electrochemically intercalating different amounts of Lithium into VOx-NTs.

2. EXPERIMENTAL SECTION

2.1. Synthesis. Vanadium oxide nanotubes were synthesized using the hydrothermal procedure similar to that described in refs 13 and 21. A solution of vanadium (V^{5+}) triisopropoxide [$VO(iOPr)_3$] and a primary amine ($CH_3-(CH_2)_{11}-NH_2$) in a molar ratio of 2:1 in absolute ethanol (3 mL per g of [$VO(iOPr)_3$]) was stirred under nitrogen atmosphere for 1 h. This resulted in a light-yellow solution of alkoxide-amine adduct. This was hydrolyzed with water (5 mL per g of [$VO(iOPr)_3$]) while stirring. The adduct was continually stirred and aged at room temperature for ~4 days, turning dark orange. The hydrothermal reaction of this composite in an autoclave at 180 °C for 8 days yielded a black powder of VOx-NTs that was then washed with ethanol and hexane and dried at 85 °C in vacuum for ~30 h. The VOx-NTs have been characterized using scanning electron microscopy (SEM) in a FEI Nova-Nanosem-200 and transmission electron microscopy (TEM) in FEI Tecnai F30.

2.2. Electrochemical Measurements. Electrode materials have been prepared from a mixture of VOx-NTs, 10 wt % of Carbon SP (Timcal, LTd, Bodio, Switzerland), and 5% of PVDF binder (Solexis, Tavaux Cedex, France). Approximately 10 mg of mixture pressed in pellet was placed in two-electrode Swagelok-like cells. The cells were assembled inside the glovebox under Ar-atmosphere (O_2/H_2O < 2 ppm). In the two-electrode cell, lithium metal was used as negative electrode and VOx-NTs as positive electrode. The two parts were separated by two sheets of Whatman borosilicate glass fiber, soaked in electrolyte to maintain good ionic conductivity and well-physical separation of the two electrodes. The electrolyte used was 1 M solution of $LiPF_6$ salt in ethylene carbonate (EC)/dimethyl carbonate (DMC) mixture 1:1 in weight (Ferro Corporation, Ohio, U.S.A.). Cyclic voltammetry and potentiostatic measurements were performed using a VMP multichannel controller (Princeton Applied Research, Illingen, Germany). The experiments were performed at fixed temperature of T = 25 °C.

2.3. Magnetic Measurements. Electrochemical (potentiostatic) techniques were used to obtain lithium doped VOx-NTs, i.e. Li_xVOx-NTs with the particular Li-content x = 0.05, 0.1, 0.155, 0.2, and 0.4. The magnetic properties of both undoped and doped VOx-NTs were studied. For this purpose, a MPMS-XL5 SQUID magnetometer (Quantum Design, Darmstadt, Germany) was applied for investigations of the field dependence of the magnetization at constant temperatures. The ^{7}Li NMR experiments were carried out with a Tecmag pulse solid-state NMR spectrometer in a field of 4 T.

3. RESULTS AND DISCUSSION

The morphology of the synthesized VOx-NTs was investigated by means of SEM and TEM. In Figure 1, the multilayer tubular morphology is illustrated. In general, the tubes have inner diameters between 20 and 30 nm and the outer diameters are varying between 50 and 100 nm.

3.1. Cyclic Voltammetry. In the following, electrochemical studies of different samples (1−5) of VOx-NTs are described. Although the synthesis conditions of all five samples have been very similar, small deviations in the hydrothermal synthesis process yield subtle but visible differences in the electrochemical behavior.

The cyclic voltammograms for the first cycle for VOx-NT (1) are shown in Figure 2. The starting potential was around 3.2 V. From this value, the potential was cycled between 1.8 and 3.5 V using different scan rates. First, the cell was discharged (going from 3.2 to 1.8 V) using scan rates of 0.2 and 0.05 mV/s, respectively. As expected, the overall behavior is similar for the two scan rates but the current is larger in case of the faster sweeping rate. Upon discharging, that is, Li-intercalation, two reduction peaks indicating two different electron transfer reactions are encountered at 2.42 and 2.09 V, respectively. During the cell charging, one finds two peaks at 2.83 and 3.17 V. In general, the data shown in Figure 2 suggest that the discharged material in the cathodic sweep was reversibly charged during the anodic sweep, or in other words that the electrons transfer process is chemically reversible. This electron transfer appears at a specific voltage due to redox reaction when the reduction of V^{5+} to V^{4+} takes place (or V^{4+} to V^{3+}). Note that at 2.73 V, the cathodic scan presents a shoulder, which is probably associated with the anodic peak at 2.64 V. For VOx-NT (1) the initial discharge capacity is 140 mAh/g when the current was swept with a scan rate of 0.05 mV/s.

Cyclic voltammograms for the materials VOx-NT (2), (3), (4), and (5) performed with 0.02 mV/s are shown in Figure 3. The CVs are generally similar with reduction/oxidation peak pairs in the same potential region, but there are small differences between the materials. For each batch, four consecutive CV cycles were performed (only the first circle is shown). For all experiments, the cutoff potentials were 1.8 and 4 V, always starting with the discharge of the material. The starting potentials were around (3.2 ± 0.2) V, indicating a stable behavior over the mounting procedure of the electrode materials.

In the following, subtle differences between the four materials are discussed. For VOx-NT (2) upon discharge the electron transfer due to reducing of V^{5+} to V^{4+} occurs at 2.83 V as displayed by the very pronounced reduction peak. Upon further

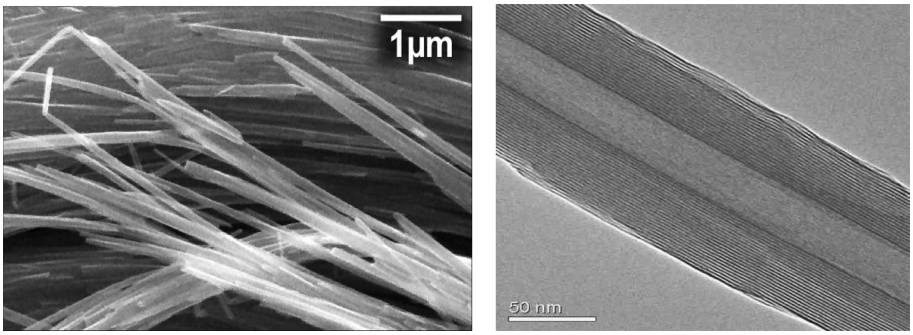

Figure 1. Tubular morphology of VOx-NTs proven by SEM (left) and TEM (right) studies.

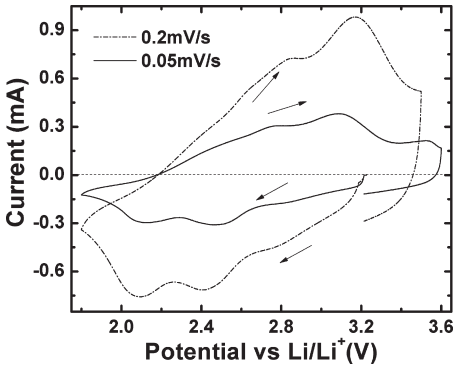

Figure 2. Cyclic voltammogram for VOx-NT (1) performed with scan rate of 0.2 and 0.05 mV/s, respectively. The arrows indicate the discharging and charging of the material.

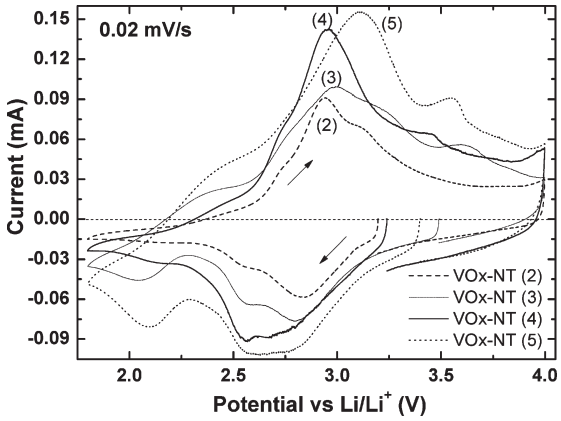

Figure 3. Cyclic voltammograms for VOx-NT (2), (3), (4), and (5) performed with a scan rate of 0.02 mV/s. The arrows indicate the discharge and charge of the material.

cycling, this value slightly shifts to higher potentials. The corresponding oxidation peak is situated at 2.94 V. Both peaks exhibit shoulders which are most probably related and disappear upon cycling. The peaks are broader in VOx-NT (3) but at very similar potentials: the reduction peak is centered on 2.8 V (anodic peak at 2.99 V) and shifts to 2.82 V during further cycling. The current peak intensities vary more over cycling than those in VOx-NT (2). Again, the shoulder at 2.57 V completely disappears already in the second cycle of this experiment and both the reduction and oxidation peaks narrow upon cycling. For VOx-NT (4) and (5), the first reduction occurs at a lower potential than in the other materials, that is, at 2.56 and 2.62 V, respectively. Here, there are stronger effects of cycling that yield a shift to 2.82 V (2.9 V) in the fourth cycle. The oxidation peaks are found at 2.96 and 3.1 V. Note, that the oxidation peak is narrower than the cathodic one. The peak around 2 V is attributed to possible reduction of V^{4+} to V^{3+}, as also valid for VOx-NT (3).

Figure 4 illustrates a resume of the specific capacity values for VOx-NTs studied in this work taken from CV experiments. The highest initial discharge capacity is found for VOx-NT (3) and (5), which displays values of 145 mAh/g. The specific capacities decrease upon cycling, for example, to 114 mAh/g in batch (3). In contrast, VOx-NT (4) has 123 mAh/g initial discharge capacity that increases to 153 mAh/g in the second cycle.

The electrochemical behavior presented in Figure 2 (for VOx-NT (1)) and Figure 3 (for VOx-NT (2−5)) differs, although all materials have been synthesized in a very similar way. In addition to the effects of the synthesis procedure, aging plays an important role in VOx-NTs since the nanoscaled morphology implies chemical reactivity. Moisture, that is, water is known to reduce[25] the V^{5+} to V^{4+}, and therefore in the studied materials the mixed vanadium valence is possibly different from the value of 4.4^{+} suggested in refs 11 and 22. It is also possible that if extra water enters in the VOx-NTs, the available space for Li intercalation decreases, controlling their electrochemical properties.

Also different amounts of the amines influences the mixed valence of the V in the VOx layers thereby causing possible differences between similarly prepared materials. In addition, the surfactant can reduce the available surface area for redox reactions and can also form aggregates that would block the Li ions access to intercalation sites in the VOx layers. These effects can be smaller if the nanotubes have cracks in the walls. This atomic scale disorder would give a higher accessibility for Li ions and thus an increased specific capacity. Different sizes of the nanotubes can give different Li diffusion distances. Short distances give high surface area and this lowers the Li^{+} insertion rate density in the intercalation process, which in turn, postpones the decreasing of the capacity.

In the following, the differences in the electrochemical behavior of the materials will be discussed. The CV of VOx-NT (1) presented in Figure 2 is similar to that of template free VOx-NT shown in ref 10, raising the question of amines role in this material. In general, the amines are expected to cause a partial passivation of the nanotubes.[10] However, the electron transfer reactions present in VOx-NT (1) occur at similar potential as in Ca-exchanged VOx-NT[20] indicating that in the first case the amines did not significantly avert the lithium intercalation process.

dx.doi.org/10.1021/jp109327x |J. Phys. Chem. C 2011, 115, 5265–5270

As described above for batches (2−5), there are variations of the anodic and cathodic peak positions. It is straightforward to assign the differences to structural deformation, aging of the material, or crystallinity loss during cycling. A resistance of the reduced VOx layers to readopt their original structure may also generate differences.[20] The most obvious difference in the CVs of the materials is the presence of additional clear features around 2 V in the cathodic scans of VOx-NT (3) and (5) and at 3.7 V in the anodic scan (5). The cathodic peaks might indicate the second reduction process V^{4+} to V^{3+} of the materials, although usually potentials lower than 2 V are needed for this electron transfer.[16] Peak broadening in the second cycle compared to the first one, as mentioned for VOx-NT (3), can be explained by structural rearrangements of the electrochemical active VOx layers after the first cycle. Clear modifications of an $I-V$ curve in the second cycle compared to the first one suggest that irreversible transformations occur during the initial Li insertion process. In the following cycles, neither substantial change in the peak potential value nor in the curve shape is present, indicating quasi redox-reversible intercalation process for these cycles.

Another interesting feature is the observation of a very broad, nearly plateaulike reduction peak in VOx-NT (5). One might speculate that in this region the broadening and overlapping of the reduction peak itself and the shoulder seen in VOx-NT (2) and (3) yield the plateaulike behavior. Broadening is a typical result of a more disordered structure. For example, in VOx-NT (3) the fact that the second cycle is different from the first one indicates a structural rearrangement after the first cycle. This is even more pronounced in VOx-NT (5). Here, already the peaks in the charging and discharging cycle exhibit different widths so Li-insertion and extraction is governed by different mechanism.

The electrochemical behavior found for VOx-NTs (2−5) is very similar to that described by Sun et al. for defect rich Na^+-exchanged VOx-nanorolls that have been synthesized by a similar method,[19] indicating a possible amine deficiency in the first case. The hydrothermal step during the synthesis of the VOx-NTs is crucial for the electrochemical properties of this material. It has been shown that a larger amount of amines remained in between the VOx layers after a Na-exchanged process induces different electrochemical behavior[19] by blocking the Li ion access to sites in the VOx layers and therefore affecting their electrochemical properties.

The specific capacity behavior upon cycling displayed by the data in Figure 4 is a feature also found in other VOx nanostructures (for example, in refs 10 and 19). It is typically caused by amorphization or other structural changes that appear over cycling. In the case of VOx-NTs at hand, Li might remain between the VOx layers so that it is not completely deintercalated upon charging, thereby lowering the reversible capacity and decreasing the number of available sites for Li ions.

VOx-NTs studied in this work have slightly superior specific capacity values than VOx-NTs with template found in the literature. For $VO_{2.45}$ $(TEMP)_{0.34}$ (TEMP = $C_{16}H_{33}NH_2$), the initial specific discharge capacity amounts to 120 mAh/g. If the templates are removed, values of 180 mAh/g are found.[10] Interestingly, the specific capacity values described in this work are comparable to those for different ion-exchanged VOx-NTs, although the synthesis methods are different.[16] The higher values of specific discharge capacities for templated VOx-NTs in the present work indicates that the amines did not completely block the available sites for the Li intercalation/deintercalation process.

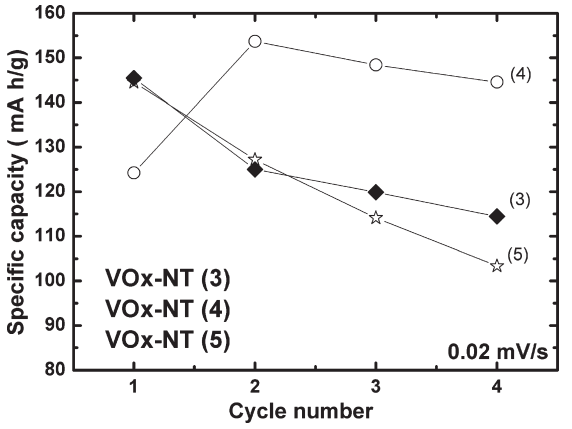

Figure 4. Specific discharge capacity as obtained from the CVs shown in Figure 3.

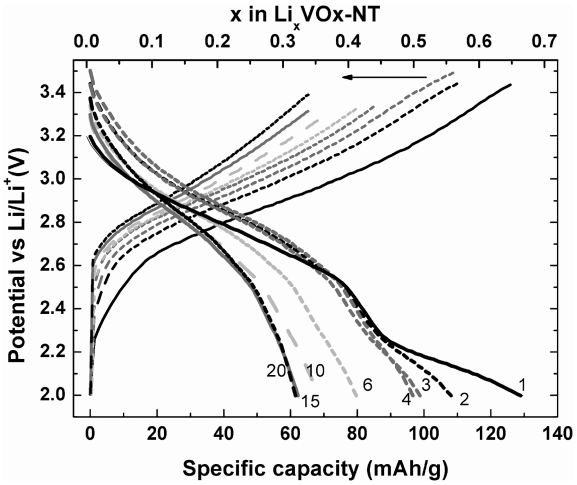

Figure 5. Potential versus specific capacity and the Li amount x in Li_xVOx-NT obtained from potentiostatic studies on VOx-NT (3). The scans have been performed at rate $C/100$ (I = 0.027 mA). The arrow indicates numbering of cycles from 1 to 20.

3.2. Potentiostatic Measurements. Figure 5 shows potentiostatic data on VOx-NT (3) where the potential of the electrochemical cell was maintained constant until the current reached a previously established limit (C/t rate). Subsequently, the potential was decreased (when discharging) or increased (when charging) using 5 mV steps. The rate used was C/100, that is, complete discharge in 100 h. The curves show slight changes of the slope at potential values of 2.4, 2.6, and 2.8 V. The absence of an obvious plateau in these curves is the clear indication of a monophasic Li intercalation process, that is, there is no discrete phase formation during cycling. Interestingly, the first three cycles of the potentiostatic experiment are different from the following ones. This difference may arise from different intercalation processes present in the first three cycles compared to the later ones. A similar conclusion might be drawn from differences between the first and the other cycles in CV experiments. One possible scenario is that in the beginning, Li^+ ions are inserted in a quite disordered way between the VOx-layers (valid for cycles 1 to 3). In a presumably second step of the intercalation process, the Li^+ ions might then diffuse to find favorable sites in the interlayer spaces of the structure, affecting the VOx structure (valid from cycle 4 onward).

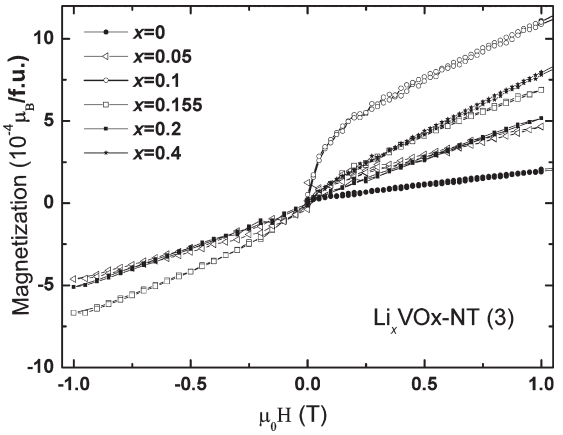

Figure 6. Field dependence of the magnetization of Li_xVOx-NT (3) at 300 K for x = 0, 0.05, 0.1, 0.155, 0.2 ,and 0.4.

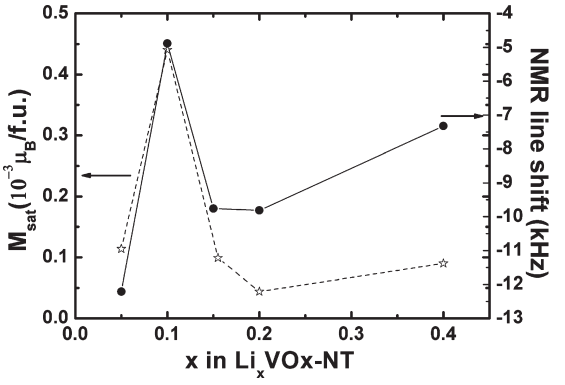

Figure 7. Doping dependence of the saturation magnetization (left-hand side) and of the ^{7}Li- NMR line shift (right-hand side) for Li_xVOx-NTs (3).

The data in Figure 5 again allow following the effect of cycling on the specific discharge capacity. In the first cycle, it amounts to 130 mAh/g, which corresponds to a Li-intercalation level of 0.66 (cf. upper abscissa of Figure 5). This value decreases with cycling and it reaches a roughly constant value after the tenth cycle. This decrease can be the result of side reactions, or maybe Li ions sites are blocked by amines. Note that due to a smaller potential window used for the potentiostatic experiments, the specific capacity is slightly lower than in the CVs. Using potentiostatic experiments, it has been shown that the Li-intercalation process is a monophasic process with no drastic structural changes of the studied material (see comments on Figure 5). The values of the specific capacities found here are higher than those found for other template VOx-NTs presented in literature, but smaller than for template-free nanotubes. A previous study has shown that the structure of mixed-valent vanadium oxide nanotubes is stable against electron transfer upon Li-doping.[23] Generally, it is known that the nanotube morphology is preserved after cycling.[17,26]

3.3. Magnetic Properties. Using electrochemical methods as described above, Li was intercalated in VOx-NTs in order to study the magnetic properties of Li_xVOx-NTs as a function of electronic doping for $0.05 \leq x \leq 0.4$. The magnetic properties of undoped VOx-NTs have been already shown in detail elsewhere.[22] In the pristine material, vanadium ions have a mixed valence state, with an average valence count of ~4.4+ (i.e., $x \sim 2.2$ in VOx-NT).[11] Hence, approximately 60% of the V sites exhibit magnetic V^{4+} ions ($3d^1$, S = 1/2) and 40% nonmagnetic V^{5+} ions ($3d^0$, S = 0). The magnetic properties reflect the appearance of individual spins, antiferromagnetic dimers, and trimers.[22] However, upon Li-doping the magnetic properties are completely changed, that is, the spin gap disappears in electrochemically doped VOx-NTs and a ferromagnetic-like response evolves at room temperature at the doping level x = 0.1.[24]

In general, by applying an electrical voltage, lithium is inserted in the crystal structure and the valence of the transition metal ion, that is, the number of electrons in the 3d shell of the V ions, is altered. Doping with electrons is expected to reduce V^{5+} into V^{4+} and therefore to increase the number of the magnetic sites, that is, V^{4+} (S = 1/2). An increase of the number of magnetic sites is indeed observed with our experimental data. In addition, however, there is a clear evolution of a ferromagnetic-like response upon doping visible in Figure 6. Here, the field dependence of the magnetization measured at room temperature (T = 300 K) for Li_xVOx-NT is shown. For the undoped material, the field dependence of the magnetization has a linear behavior as expected for a paramagnet. Clear nonlinear field dependence in applied fields up to 0.2 T appears at x = 0.05, gets most pronounced at x = 0.1, and vanishes at higher doping levels.

Our data hence provide clear evidence that Li-doping drastically changes the magnetic interaction between the vanadium magnetic moments. While the pristine material is governed by antiferromagnetic dimers and trimers, room temperature ferromagnetism is present in $Li_{0.1}VOx$-NT. The detailed analysis of ESR, μSR, and NMR enabled us to conclude that the ferromagnetic-like response in $Li_{0.1}VOx$-NT is associated with the formation of small ferromagnetic clusters.[24] Interestingly, the data in Figure 6 imply a particular role for the doping level x = 0.1 where additional ferromagnetic-like contribution is most pronounced. A quantitative analysis of the nonlinear feature in M (B) is done by subtracting the linear high-magnetic field dependence of the magnetization that allows extracting the saturation moment of the ferromagnetic-like response. The result of this analysis is shown in Figure 7. The data clearly show the particularly large effect at x = 0.1 as well as a strongly nonmonotonous doping dependence. The particular role of this doping level is corroborated by the shift of the ^{7}Li- NMR line (Figure 7). The main factor affecting a monotonic growth of the NMR frequency of this line upon Li doping is the hyperfine interaction with the vanadium d-electrons. The increase of the Li doping provides additional electrons to the matrix thus, progressively reducing the number of nonmagnetic V^{5+} ($4d^0$, S = 0) ions and increasing the number of magnetic V^{4+} ($4d^1$, S = 1/2) ions containing one electron on the d-shell. Apparently, the origin of the sharp line shift for the $Li_{0.1}VOx$-NT sample is different. ^{51}V NMR (not shown here) does not indicate any anomalies that could be related to the excess of the amount of the magnetic V^{4+} sites at this particular doping level. Therefore, the ^{7}Li NMR line shift can be only due to the internal magnetic field at the position of the lithium nuclei.[24] Thus an "extra" displacement of the lithium line of the $Li_{0.1}VOx$-NT sample to a higher frequency (Figure 7) gives evidence for the appearance of the static (at least on the NMR time scale) ferromagnetically ordered areas around the Li sites that create an internal field on all Li nuclei in the sample.

The unexpected occurrence of room-temperature ferromagnetism upon electrochemical lithium doping of VOx-NTs has been described in more detail in ref 24 for Li_xVOx-NTs (1). For both Li_xVOx-NTs (1) and Li_xVOx-NTs (3), it appears that the

Li concentration $x = 0.1$ represents the optimal doping level for the room temperature ferromagnetism hinting at a delicate balance between electronic and structural factors. Although our studies exhibit differences in the electrochemical response, the evolution of HTFM appears robust against small deviations, that is, in morphology. High-temperature ferromagnetism attributed to ferromagnetic clusters formation has been also found in nanoscale diluted magnetic semiconductors (DMS)[27,28] and ascribed to collective polaronic effects.[29,30] As discussed in ref 24, a polaronic scenario may be relevant for VOx-NTs as well suggesting that an appropriate tuning of the electronic, structural, and magnetic properties of transition metal oxide nanostructures by lithium intercalation may indeed result in high-temperature ferromagnetism.

4. CONCLUSIONS

In the present work, mixed valence VOx-NTs have been characterized both by electrochemical and magnetic methods. It is concluded that the electrochemical behavior of the VOx-NTs is very sensitive to the preparation conditions. Different surfactant content and/or amount of water could influence the electrochemical properties of VOx-NTs. Different nanotube sizes, as well as aging of the material can be another source for differences in electrochemical behavior of similarly prepared VOx-NTs. The electrochemical properties of the studied compounds are superior to other template-VOx-NTs. Using electrochemical techniques, the charge carrier density in VOx-NT can be modified and controlled via lithium intercalation into the structure. Room-temperature ferromagnetism has been found for the optimal Li doping level $Li_{0.1}$VOx-NTs in two different batches, although being distinct from the electrochemical point of view.

AUTHOR INFORMATION

Corresponding Author
*E-mail: a.popa@ifw-dresden.de.

ACKNOWLEDGMENT

Collaboration and discussions with C. Masquelier and M. Morcrette are gratefully acknowledged. Work has been supported by the Deutsche Forschungsgemeinschaft (KL 1824/2 and BU-887/13-1) by BMBF within the initiative LIB 2015 (Nachwuchsgruppe 03SF0340) and by the Russian Foundation for Basic Research (08-02-91952-NNIO-a).

REFERENCES

(1) Poizot, P; Laurelle, S; Grugeon, S; Dupont, L; Tarascon, J.-M. *Nature* **2000**, *407*, 496.
(2) Arico, A S.; Bruce, P; Scrosati, B.; Tarascon, J.-M.; Van Scharlkwijk, W. *Nat. Mater.* **2005**, *4*, 366.
(3) Armand, M; Tarascon, J.-M. *Nature* **2008**, *451*, 652.
(4) Park, M-H; Kim, M G; Joo, J; Kim, K; Kim, J; Ahn, S; Cui, Y; Cho, J. *Nano Lett.* **2009**, *9*, 3844.
(5) Yang, Y; Xie, C.; Ruffo, R; Peng, H; Kim, D K; Cui, Y. *Nano Lett.* **2009**, *9*, 4109.
(6) Zhang, H; Gao, X. P.; Li, G. R.; Yan, T. Y.; Zhu, H. Y. *Electrochim. Acta* **2009**, *53*, 7061.
(7) Tenne, R. *Nat. Nanotechnol.* **2006**, *1*, 103.
(8) Bae, C.; Yoo, H.; Kim, S.; Lee, K.; Kim, J.; Sung, M. M.; Shin, H. *Chem. Mater.* **2008**, *20*, 756.
(9) Ortiz, G. F.; Hanzu, I.; Djenizian, T.; Lavela, P.; Tirado, J. L.; Knauth, P. *Chem. Mater.* **2009**, *21*, 63.
(10) Spahr, M. E.; Stoschitzki-Bitterli, P.; Nesper, R.; Haas, O.; Novák, P. *J. Electrochem. Soc.* **1999**, *146*, 2780.
(11) Liu, X.; Täschner, C.; Leonhardt, A.; Rümmeli, M. H.; Pichler, T.; Gemming, T.; Büchner, B.; Knupfer, M. *Phys. Rev. B* **2005**, *72*, 115407.
(12) Muhr, H.-J.; Krumeich, F.; Schönholzer, U. P.; Bieri, F.; Niederberger, M.; Gauckler, L. J.; Nesper, R. *Adv. Mater.* **2000**, *12*, 231.
(13) Krumeich, F.; Muhr, H.-J.; Niederberger, M.; Bieri, F.; Schnyder, B.; Nesper, R. *J. Am. Chem. Soc.* **1999**, *121*, 8324.
(14) Reinoso, J. M.; Muhr, H.-J.; Krumeich, F.; Bieri, F.; Nesper, R. *Helv. Chim. Acta* **2000**, *83*, 1724.
(15) Dobley, A.; Ngala, K.; Yang, S.; Zavalij, P. Y.; Whittingham, M. S. *Chem. Mater.* **2001**, *13*, 4382.
(16) Nordlinder, S.; Lindgren, J.; Gustafsson, T.; Edström, K. J. *Electrochem. Soc.* **2003**, *150*, E280.
(17) Nordlinder, S.; Edström, K. J.; Gustafsson, T. *Electrochem. Solid-State Lett.* **2001**, *4*, A129.
(18) Mai, L.-Q.; Chen, W.; Xu, Q.; Peng, J.-F.; Zhu, Q.-Y. *Chem. Phys. Lett.* **2003**, *382*, 307.
(19) Sun, D.; Kwon, C. W.; Baure, G.; Richman, E.; MacLean, J; Dunn, B.; Tolbert, S. H. *Adv. Funct. Mater.* **2004**, *14*, 1197.
(20) Nordlinder, S.; Nyholm, L.; Gustafsson, T.; Edström, K. *Chem. Mater.* **2006**, *18*, 495–503.
(21) Krusin-Elbaum, L.; Newns, D. M.; Zeng, H.; Derycke, V.; Sun, J. Z.; Sandstrom, R. *Nature* **2004**, *431*, 672.
(22) Vavilova, E.; Hellmann, I.; Kataev, V.; Täschner, C.; Büchner, B.; Klingeler, R. *Phys. Rev. B* **2006**, *73*, 144417.
(23) Hellmann, I.; Täschner, C.; Klingeler, R.; Leonhardt, A.; Büchner, B.; Knupfer, M. *J. Chem. Phys.* **2008**, *128*, 224701.
(24) Popa, A. I.; Vavilova, E.; Arango, Y.; Hellmann, I.; Kataev, V.; Täschner, C.; Klauss, H. H.; Maeter, H.; Luetkens, H.; Büchner, B.; Klingeler, R. *Euro. Phys. Lett.* **2009**, *82*, 57002.
(25) Kweon, H; Lee, K. W.; Lee, E. M.; Park, J; Kim, I. M.; Lee, C. E. *Phys. Rev. B* **2007**, *76*, 045434.
(26) Li, X.; Li, W; Ha, M; Chen, J. *J. Electrochem. Soc.* **2007**, *154*, A39.
(27) Radovanovic, P; Gamelin, D. R. *Phys. Rev. B* **2003**, *91*, 157202.
(28) Xing, G. Z.; Yi, J. B.; Tao, J. G.; Liu, T.; Wong, L. M.; Zhang, Z.; Li, G. P.; Wang, S. J.; Ding, J.; Lum, T. C.; Huan, C. H. A.; Wu, T. *Adv. Mater.* **2008**, *20*, 3521.
(29) Kaminski, A.; Das Sarma, S. *Phys. Rev. Lett.* **2002**, *88*, 247202.
(30) Durst, A. C.; Bhatt, R. N.; Wolff, P. A. *Phys. Rev. B* **2002**, *65*, 235205.